Int J Earth Sci (Geol Rundsch) (2017) 106:1257–1276
DOI 10.1007/s00531-016-1333-0

ORIGINAL PAPER

Composition and sediment dispersal pattern of the Upper Triassic flysch in the eastern Himalayas, China: significance to provenance and basin analysis

Chaokai Zhang[1] · Xianghui Li[1] · Frank Mattern[2] · Qinggao Zeng[3] · Guozheng Mao[3]

Received: 28 December 2015 / Accepted: 13 April 2016 / Published online: 3 May 2016

Abstract The paleogeography and basin type of Upper Triassic flysch (Langjiexue Group) in the eastern Himalayan Orogen are disputed. In order to shed new light on the flysch's origin, we applied different sedimentological methods. Assemblages of heavy minerals and clastic components of sandstones were utilized to determine the primary depositional composition. Heavy mineral indices, S/M ratios (thickness of sandstone + siltstone "S" versus slate/mudrock "M"), and paleocurrent data were combined to reveal the sediment dispersal pattern and the location of the source areas. In the analyzed sandstones, heavy minerals such as zircon, rutile, tourmaline, apatite, and anatase are most common, and zircon is predominant (most over 60 %). ZTR values range from 60 to 98 % and systematically increase southward. As a provenance-sensitive parameter, RuZi values vary in large magnitude and are significantly higher in both the east and west (>20 %) than in the center. The majority of S/M ratios decrease from north to south, suggesting an overall decrease in grain size to the south. Paleocurrent directions vary between 120° and 270° (main vector 205°, and 185° after 20° counterclockwise correction), displaying a radial-curved pattern. Variable heavy mineral assemblages indicate different sources, and the sandstones fall in the "recycled" and "mixed-arc orogeny" fields of Dickinson triplots, together supporting the view of multiple sources. Results of the ZTR values, S/M ratios, and paleocurrent directions illustrate a dispersal pattern, corresponding to a submarine fan system. The provenance and submarine fan dispersal pattern along with the basin configuration (deep basin with oceanic affinities) suggest that the Langjiexue Group accumulated in a remnant basin between Lhasa, Greater India, and Australia, where the sediments dispersed into the basin toward the developing orogen/suture zone and not away from the orogen, challenging the provenance direction for the traditional remnant basin model.

Keywords Sediment dispersal · Provenance · Remnant basin · Himalayan orogeny · Upper Triassic · Tibet

Introduction

The stratigraphic Shannan Terrane (Li et al. 2016), in the northeast of the Himalayan Orogen of southeastern Tibet, is composed of the Upper Triassic flysch (Langjiexue Group). It is extensively exposed in an area of over 40,000 km^2 south to the Yarlung Zangbo Suture Zone (YZSZ) (Fig. 1). The Upper Triassic has been interpreted either as deep-sea sediments of the Tethyan Himalaya (Yu and Wang 1990), i.e., in the northern Indian passive margin (e.g., Wang 1983; Yin and Harrison 2000; Dunkl et al. 2011), or as an accretionary prism (Zhou et al. 1984; Pan et al. 2004; Wang et al. 2013) within the mélange belt of the YZSZ to the west of Xigaze (TBGMR 1993, 1997). These views are challenged by the recent discovery of southward paleocurrent directions in Qonggyai County (Li et al. 2003a; Xu

Electronic supplementary material The online version of this article (doi:10.1007/s00531-016-1333-0) contains supplementary material, which is available to authorized users.

✉ Xianghui Li
leeschhui@126.com

[1] State Key Laboratory of Mineral Deposit Research, School of Earth Sciences and Engineering, Nanjing University, No. 163, Xianlin Avenue, Nanjing 210046, Jiangsu, China

[2] Earth Science Department, College of Science, Sultan Qaboos University, PO Box 36, Muscat, Sultanate of Oman

[3] The 1st Geology Survey of Tibet, Lhasa 850000, Tibet, China

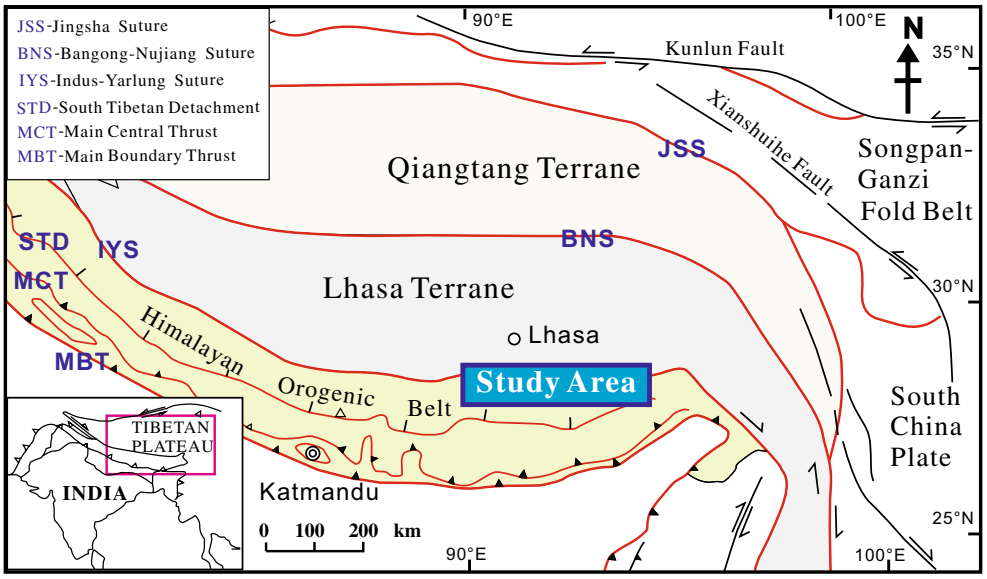

Fig. 1 Tectonic zonation of the Himalaya and the Tibet Plateau (simplified after Searle et al. 2006), showing the location of the study area. *Insert* at *down-left corner* is the geotectonic sketch of South Asia

et al. 2009). Subsequent studies supported the idea of one or more northern sources (e.g., Li et al. 2003b, 2004; Dai et al. 2008; Xu et al. 2009, 2011; Zeng et al. 2009; Li et al. 2010, 2014; Webb et al. 2013; Zhang et al. 2015). Also a derivation from either the Lhasa Terrane or a possible independent continent in the Neo-Tethys Ocean was proposed (e.g., Li et al. 2004) and supported (Li et al. 2010, 2014; Webb et al. 2013; Zhang et al. 2015), and a rift basin was suggested as well (Li et al. 2010, 2014; Webb et al. 2013).

The interpretation of a rift basin is contrary to the recycled orogenic setting of the source regions (Li et al. 2004; Xu et al. 2009; Li et al. 2010). Also, the proposition of multiple sources supplying the basin (Li et al. 2016) blackballs the rift basin model. It also needs to be mentioned that data of former works were only locally collected from two locations (Qonggyai and Rinbung Counties), which seems unrepresentative of the entire study area. Thus, it is necessary to present more new sedimentological details from the entire region, relying on additional methods in order to better understand the sedimentology in clastic composition, dispersal, and provenance as well as the basin type of the Langjiexue Group except for the depositional environments and lithofacies (Zhang et al. 2015).

By applying different sedimentological methods, a great number of data were obtained, aiming to clarify the dispersal pattern of the Langjiexue Group, to test the idea of multiple sources and to pinpoint the flysch's paleogeographic position within the Tethys Ocean, possibly enabling us to improve the understanding of the subsequent Indo-Asian collision and the geological/tectonic evolution of southern Tibet.

Geological field investigations and sampling of the Langjiexue Group have been undertaken in the entire outcrop area from Rinbung in the west to Zara Village of Lhunze County in the east (Fig. 2; Table 1). Firstly, the provenance of Langjiexue Group was probed through analyses of heavy minerals and clastic composition. Then, the ZTR index, the paleocurrent direction, and lithological statistics in thickness were combined to analyze depositional compositions and sediment dispersal patterns. Finally, the provenance and basin type are tentatively pinned down.

Geological setting

From the Himalaya, the tectonic belts in southern Tibet northward are the Lesser Himalaya, High (crystalline) Himalaya, Tethyan Himalaya, YZSZ, Xigaze Forearc Basin, and the Gangdese Arc (Gansser 1991). The Tethyan Himalaya is subdivided into the southern subbelt with shallow marine deposits and the northern subbelt with deep marine deposits (Yu and Wang 1990; Wang et al. 1996, 2000). The Upper Triassic Langjiexue Group has been assigned to the northern Tethyan Himalaya, cropping out south of the eastern part of the YZSZ in the Shannan area of southern Tibet (Figs. 1, 2). The thickness of the group varies from 500 m to 2000 m (Zhang et al. 2015), likely up to ~3000 m.

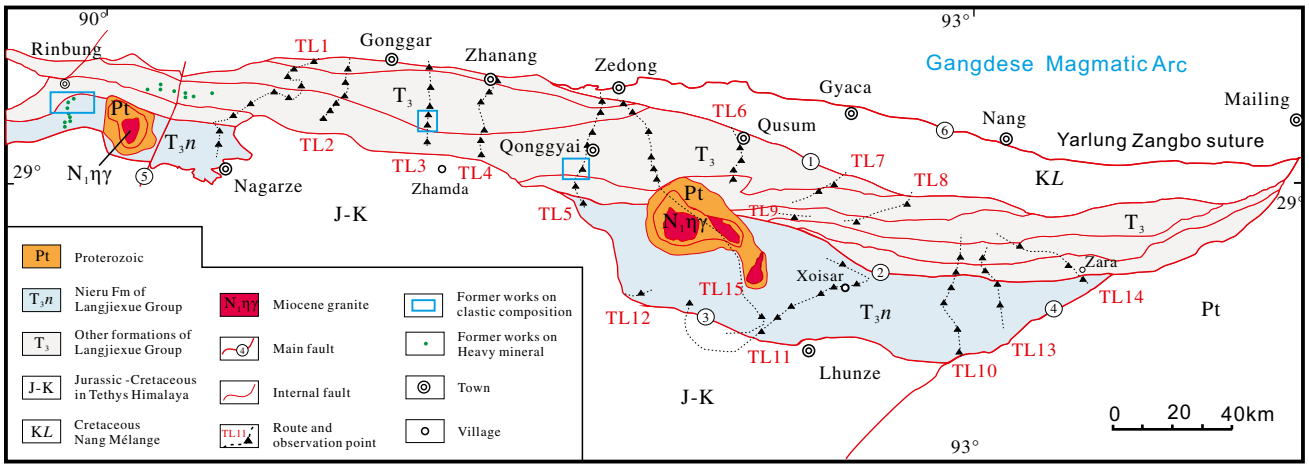

Fig. 2 Geological sketch of Shannan Prefecture, southern Tibet (drawn and modified from Pan et al. 2004), showing the distribution of the Upper Triassic Langjiexue Group, field investigation routes and observation sections. Former works on heavy mineral and clastic composition (Li et al. 2004; Zeng et al. 2009; Li et al. 2010; Xu et al. 2011) are marked by *dot* and *rectangle*, respectively. Details of investigation routes and observation sections refer to Table 1. ① Great Counter Thrust; ② Qiongduojiang–Zara Fault; ③ Rinbung–Zhamda–Lhunze Fault; ④ Cona–Mailing Fault; ⑤ Yangbajing–Qiongdui Fault; ⑥ Sangri–Gyaca–Nang Fault

The Langjiexue Group is preliminarily referred to as the "Shannan Terrane" and "Shannan Basin" when the tectonic and paleogeographic relationships with other terranes and sedimentary basins are discussed (Li et al. 2016). It is mainly confined by three thrust faults: the Great Counter Thrust (GCT) in the north, the Rinbung–Zhamda–Lhunze Fault in the south, and Cona–Mailing Fault to the east (Fig. 2). The sedimentary strata were metamorphosed to variable degrees, increasing eastward, reaching greenschist and amphibolite facies toward the metamorphic core of the thermal dome center, which is occupied by the Cenozoic granitic pluton (e.g., Dunkl et al. 2011; Montomoli et al. 2008). The metamorphism started during the Early Cretaceous was attributed to diabase dyke emplacement and mainly completed in three stages after 44 Ma (Aikman et al. 2008; Zhu et al. 2009; Dunkl et al. 2011). Folding and thrusting are associated with metamorphism, which could be the result of hinterland propagation of deformation. Furthermore, ~20° clockwise vertical-axis rotations could have taken place during the Early Miocene as shown by different orientations of the magnetic foliation (Antolin et al. 2011). In the past, the northern part of the Langjiexue Group formally consisted of the Songre Fm. (Formation), Jiangxiong Fm., Jiedexiu Fm., and Zhangcun Fm., which are difficult to distinguish in the field. Recently, the Nieru Fm. (to the south of former Langjiexue Group, Fig. 2) was suggested to belong to the Langjiexue Group for their many similarities (Li et al. 2011). Because of their difficult distinction in the field, all of these formations are included in the Langjiexue Group and in our study. The group is dominantly composed of low-grade metamorphic sandstone, siltstone, and shale and must have been deposited in a deep marine environment, considering its size and turbiditic nature. The sediments represent a submarine fan system, lacking exposed inner fans (Li et al. 2003b, Zhang et al. 2015). Commonly, horizontal lamination, ripple, parallel, massive, and graded bedding can be observed. Flute casts and groove casts usually appear at the bases of coarser sandstone layers.

The age of the Langjiexue Group is determined by fossils of the bivalves *Halobia* sp., *Indopecten* sp., *Monotis* sp., *Posidonia* sp., etc. (Chen and Yang 1983; Wang et al. 1983; Chen and Ba 1986; Niu et al. 2011), and the ammonites *Arcestes* sp., *Buchites* sp., *Clasiscites* sp., *Griesbachites V*, *Indojuvavites* sp., *Palcites* sp., etc. (Wang et al. 1983; Wu 1984), together indicating a Late Triassic (Carnian–Norian) age. In addition, brachiopods, crinoids, and gastropods occasionally occur.

Methods and samples

Four fundamental methods were adopted to study the sedimentology of the Upper Triassic flysch, i.e., measurements of lithological stratigraphic thickness and paleocurrent directions, analyses of heavy minerals, and primary clastic composition (Table 1).

Heavy minerals

Sandstone samples were taken with a weight range from 0.9 to 1.5 kg. Preparation included disaggregation by a

Table 1 Details on lithological observation, sample of thin-section and heavy mineral, and paleocurrent measurement of the Upper Triassic Langjiexue Group in southern Tibet

Lithological thickness, sample for thin-section and heavy mineral									
No.	GPS (N, E)	***A***	***B***	***C***	No.	GPS (N, E)	***A***	***B***	***C***
TL1: From Nagarz to Gonggar (SW–NE)					*TL7: Gyaca (SW–NE)*				
TL1-001A	290103.8, 902357.8	1		1	TL7-01	285439.4, 922827.8	1		1
TL1-001B	290425.5, 902345.5	1		1	TL7-02	285500.5, 922844.8	1	1	
TL1-01	290701.6, 902556.8	1		1	*TL8: Gyaca (SW–NE)*				
TL1-02	290941.3, 903055.2	1		1	TL8-01	284857.2, 924000.2	1		1
TL1-03	291101.0, 903403.6	1		1	TL8-02	285155.1, 924619.6	1	1	1
TL1-04	291105.9, 903631.1	1		1	*TL9: Qusum*				
TL1-05	291234.3, 903837.5	1		1	TL9-01	284851.4, 922308.9	1		1
TL1-06	291357.3, 903758.3	1	2	1	*TL10: Lhunze (N-S)*				
TL1-07	291625.4, 903750.7	1	1	1	TL10-01	284204.8, 925644.9	1	1	1
TL1-08	291711.1, 904202.4	1	1	1	TL10-02	283853.0, 925557.4	1	1	1
TL2: From Nagarz to Gonggar (S–N)					TL10-03	283551.5, 925553.5	1		
TL2-01	290703.5, 904349.8	1	2	1	TL10-04	283244.9, 925326.2	1		1
TL2-02	290824.1, 904614.7	1	1	1	TL10-05	282815.0, 925634.4	1		1
TL2-03	291009.3, 904735.1	1		1	TL10-06	282453.7, 925804.5	1		
TL2-04	291116.9, 904924.0	1		1	*TL11: Lhunze (N-S)*				
TL2-05	291241.1, 904939.0	1		1	TL11-07	283602.2, 923114.5	1		1
TL2-06	291606.2, 904851.1	1	1	1	TL11-06	283428.9, 922811.9	1		1
TL3: From Zhamda to Gonggar (S–N)					TL11-01	283132.9, 922358.3	1	2	1
TL3-01	290213.0, 910615.8	1	3	1	TL11-02	283033.7, 922056.5	1		1
TL3-02	290422.7, 910635.7	1	2	1	TL11-03	283838.7, 921715.7	1	1	1
TL3-03	290718.2, 910636.5	1		1	TL11-04	283649.9, 923430.0	1		1
TL3-04	290949.4, 910623.1	1		1	TL11-05	283920.2, 923301.1	1	2	1
TL3-05	291304.4, 910658.4	1	1	1	*TL12: Lhunze*				
TL3-06	291525.0, 910626.4	1		1	TL12-01	283423.2, 915216.6	1		1
TL4: From Zhamda to Zhanang (S–N)					*TL13: Lhunze (N-S)*				
TL4-01	290050.4, 911832.5	1	2		TL13-02	284135.4, 930220.7	1		1
TL4-02	290255.5, 911809.0	1	1	1	TL13-03	283913.5, 930218.9	1		
TL4-03	290449.0, 911819.4	1	1	1	TL13-04	283647.7, 930452.7	1		1
TL4-04	290857.0, 911822.1	1		1	TL13-05	283253.4, 930622.2	1		1
TL4-05	291155.0, 911949.4	1		1	*TL14: Lhunze (S–W)*				
TL4-06	291420.7, 912027.5	1	1	1	TL14-01	283809.3, 932309.0	1		1
TL5: From Qoggyai to Zedong (S–N)					TL14-02	284004.1, 932210.5	1		
TL5-01	285205.3, 913812.1	1		1	TL14-03	284238.8, 930644.2	1		1
TL5-02	285458.6, 913642.3	1		1	*TL15: From Zedong to Lhunze (W–S)*				
TL5-03	285720.5, 913918.2	1		1	TL15-01	290918.7, 914708.2	1	1	
TL5-04	290147.8, 914101.5	1			TL15-02	290758.7, 914845.8	1	1	
TL5-05	290705.4, 914239.9	1	1	1	TL15-03	290522.8, 915108.4	1		
TL5-06	290827.6, 914304.8	1		1	TL15-04	290209.8, 915152.8	1		
TL5-07	290857.3, 914318.3	1		1	TL15-05	285808.2, 915322.9	1		
TL6: Qusum (S–N)					TL15-06	285558.7, 915404.1	1		
TL6-01A	285611.9, 921046.4	1			TL15-07	283018.0, 921627.2	1		
TL6-01B	285647.5, 921031.1	1				Total	72	31	55
TL6-02	285921.4, 921237.5	1		1					
TL6-03	290220.3, 921334.2	1							

Table 1 continued

Paelocurrent							
No.	GPS (N, E)	*D*	*E*	No.	GPS (N, E)	*D*	*E*
L1-4	291134.2, 903606.4	1	10	1301-1	283501.2, 922857.4	1	10
L1-5	291234.3, 903837.5	5	29	1301-2	283501.2, 922857.4	1	12
L1-6	291431.8, 903728.6	3	44	1301-3	283501.2, 922857.4	1	10
L2-1	290703.5, 904349.8	3	31	1301-4	283501.2, 922857.4	1	12
L2-1	290703.5, 904349.8	2	17	1301-5	283501.2, 922857.4	1	12
L2-2	290824.1, 904614.7	2	23	1301-6	283501.2, 922857.4	1	12
L2-3	291032.8, 904814.0	1	10	1301-7	283501.2, 922857.4	1	12
L2-4	291133.6, 904920.5	1	10	1306-1	283216.3, 920535.2	1	15
L3-1	290213.0, 910615.8	5	58	1306-2	283216.3, 920535.2	1	15
L3-2	290422.7, 910635.7	1	10	1306-3	283216.3, 920535.2	1	12
TL3-2-1	290545.3, 910646.7	1	12	1306-4	283216.3, 920535.2	1	9
L4-1	290109.5, 911822.6	4	44	1307	282623.7, 921635.8	1	12
L4-2	290320.0, 911810.3	1	12	1308	291634.6, 905347.9	1	12
L4-4	290857.0, 911822.1	2	11	1312	290559.8, 904430.5	1	12
L6-1	285647.5, 921031.1	2	10	1317	291509.0, 903720.3	1	12
L6-2	285921.4, 921237.5	2	44	P001-1	290332.0, 91155.8	1	12
L8-1	284857.2, 924000.2	1	19	P001-2	290332.0, 91155.8	1	12
L8-2	284857.8, 924015.8	4	32	P01	290247.4, 91159.5	1	8
L10-1	284204.8, 925644.9	2	40	P02	290235.6, 911511.6	1	12
L10-2	283853.0, 925557.4	3	20	P03	290117.8, 911517.1	1	2
L11-1	283602.2, 923114.5	4	10	PM004-1	290209.2, 911804.8	2	20
L11-2	283428.9, 922811.9	2	10	PM006-1	290412.5, 911512.1	2	21
TL11-3-1	283133.7, 922320.3	1	10	PM007-1	290125.7, 911527.2	3	34
L11-5	282838.7, 921715.7	1	10	PM008-1	290452.3, 911541.2	2	25
L11-6	283649.9, 923430.0	1	10	PM011-1	290300.1, 910616.7	4	45
L13-02	284259.1, 930302.1	1	10	PM015	290624.1, 910105.0	1	12
L13-03	283713.3, 930414.2	1	10	PL01	290122.1, 910530.1	1	12
					Total	92	959

A observation section for lithological S/M ratio

B samples for thin-section and clastic composition

C samples for heavy mineral

D set of paleocurrent measurement

E paleocurrent measurements at set

hydraulic crusher, followed by wet sieving and retention of the 0.2 mm, 0.1 mm, 0.05 mm size fraction, respectively (partly recommended by Morton and Hallsworth 1994). Acid treatment was avoided. Forty grams of each disaggregated sample was used for heavy mineral separation with tetrabromoethane ($C_2H_2Br_4$, $d = 2.96$ g/cm^3), magnetic touch, and dielectric techniques. All heavy mineral fractions were collected on a 5-cm^2 rectangular glass slide and selected, using a polarizing microscope. Then, the different heavy minerals (e.g., apatite, rutile, garnet, monazite, spinel, tourmaline, and zircon) were separately weighed or counted per sample (Mange and Maurer 1992).

Associations and relative ratios of heavy minerals represent parameters for the analysis of the geological environments and provenance. They are indices of provenance-sensitive heavy mineral ratios defined as the ZTR (zircon, tourmaline, rutile), ATi (apatite, tourmaline), RuZi (rutile, zircon), GZi (garnet, zircon), MZi (monazite, zircon), and CZi (chrome spinel, zircon) in weight percentage (Table 2). The definition of indices by Hubert (1962) and Morton and Hallsworth (1994, 1999) is used and c alculated in weight (for details, refer to Table RD1).

Of the heavy mineral indices, ZTR is the most commonly used one in the analysis of sediment transport

Table 2 Indices of provenance-sensitive heavy minerals from sandstones of the Upper Triassic Langjiexue Group in southern Tibet

No.		ZTR	ATi	GZi	RuZi	MZi	CZi	No.		ZTR	ATi	GZi	RuZi	MZi	CZi
1	D0145-ZHK1	73.4	73.7	25.0	28.6	0.0	0.0	37	TL3-04ZK	93.1	77.2	0.0	19.4	0.0	0.0
2	817/12ZK	78.0	62.5	0.0	12.6	0.0	0.0	38	TL3-05ZK	94.3	63.2	0.0	16.9	0.0	0.1
3	817/03ZK	91.2	62.4	0.0	65.8	0.0	0.0	39	TL3-06ZK	94.2	54.5	0.1	9.7	0.0	0.1
4	817/08ZK	83.9	76.6	2.0	13.0	0.0	0.0	40	TL4-02ZK	81.9	15.4	0.0	30.5	0.0	0.0
5	817/06ZK	45.1	86.8	0.0	0.0	0.0	0.0	41	TL4-03ZK	71.8	80.0	0.0	15.1	0.0	0.0
6	L1-7/ZK	97.1	46.2	0.0	3.7	0.0	0.0	42	TL4-04ZK	73.7	78.8	0.0	31.9	0.0	0.0
7	L1-3/ZK	97.7	63.6	0.0	4.7	0.0	0.0	43	TL4-05ZK	87.5	74.8	0.0	29.2	2.9	2.5
8	L4-9/ZK	64.4	73.6	0.0	37.5	0.0	0.0	44	TL4-06ZK	91.3	33.3	0.0	26.2	0.0	3.4
9	L4-7/ZK	94.6	50.0	0.0	7.4	0.0	0.0	45	TL5-01ZK	87.2	63.8	0.0	34.4	0.0	0.4
10	P2-3/ZK	62.5	73.5	1.9	28.6	0.0	3.8	46	TL5-02ZK	88.2	57.7	0.0	27.9	0.0	0.9
11	P2-8/ZK	87.8	77.0	0.0	48.9	0.0	0	47	TL5-03ZK	68.0	77.9	0.0	34.1	5.5	0.0
12	P1-48/HZK	88.3	100.0	0.0	16.6	0.0	0	48	TL5-05BZK	80.2	77.0	0.0	44.2	0.0	0.3
13	P1-30/ZK1	84.4	84.7	1.0	26.4	0.0	0	49	TL5-06ZK	88.9	77.1	0.0	28.6	0.0	0.1
14	P2-11/ZK	83.7	71.5	0.0	6.2	0.0	0	50	TL5-07ZK	98.2	15.7	0.0	26.4	0.5	0.2
15	P1-57/ZK	91.7	100.0	0.0	24.2	0.0	0	51	TL6-02ZK	80.3	75.8	0.0	21.1	0.0	0.0
16	P1-39/ZK	87.3	89.7	0.0	11.1	0.0	0	52	TL7-01ZK	76.2	75.0	0.0	27.4	0.0	0.0
17	P1-16/ZK	83.0	64.6	0.0	3.4	0.0	0	53	TL8-01ZK	88.8	48.3	0.0	48.8	0.0	0.4
18	TL1-001AZK	92.1	100.0	1.6	1.4	0.0	0.0	54	TL8-02ZK	72.5	93.5	0.0	24.1	0.0	0.0
19	TL1-001BZK	82.8	61.8	0.3	17.1	0.0	0.0	55	TL9-01ZK	88.7	10.9	0.0	41.7	0.0	0.0
20	TL1-01ZK	85.0	34.8	0.0	20.6	0.0	0.0	56	TL10-01ZK	72.3	5.5	37.2	37.7	0.0	0.0
21	TL01-02ZK	95.9	71.6	0.0	12.7	0.0	0.0	57	TL10-02ZK	89.2	53.8	0.0	35.0	0.0	0.0
22	TL01-03ZK	87.1	71.1	0.0	20.3	0.0	0.0	58	TL10-04ZK	89.6	42.3	0.0	41.0	0.0	0.0
23	TL01-04ZK	94.1	36.0	0.0	16.7	0.0	0.0	59	TL10-05ZK	68.1	44.4	0.0	39.1	0.0	0.0
24	TL01-05ZK	95.7	81.1	0.0	16.7	0.0	0.0	60	TL11-01ZK	92.9	63.2	0.0	20.8	0.0	0.0
25	TL01-06ZK	66.6	86.7	0.0	24.8	0.0	0.0	61	TL11-02ZK	93.9	35.5	0.0	20.0	0.0	0.0
26	TL01-07ZK	80.6	72.9	0.0	16.3	0.0	0.0	62	TL11-03ZK	90.5	28.8	0.0	21.6	0.0	0.0
27	TL01-08ZK	95.9	6.7	0.9	17.7	0.0	0.6	63	TL11-04ZK	84.6	71.9	0.0	25.7	0.0	0.0
28	TL2-01ZK	82.5	66.7	0.0	6.0	0.0	0.0	64	TL11-05ZK	77.5	82.1	0.2	25.0	0.0	0.0
29	TL2-02ZK	95.7	45.1	0.0	11.1	0.0	0.0	65	TL11-06ZK	96.7	30.3	0.7	6.8	0.0	0.0
30	TL2-03ZK	60.3	90.7	1.7	14.3	0.0	0.0	66	TL11-07ZK	97.2	60.8	0.0	21.3	0.0	0.3
31	TL2-04ZK	95.5	25.0	0.1	17.8	0.0	1.0	67	TL12-01ZK	84.7	60.9	0.0	27.1	0.0	1.4
32	TL2-05ZK	88.2	56.8	0.0	26.0	0.0	0.0	68	TL13-02ZK	93.6	11.3	0.0	28.5	0.0	0.0
33	TL2-06ZK	96.9	14.3	0.0	15.6	0.0	0.0	69	TL13-04ZK	98.7	17.4	0.0	10.5	0.0	0.5
34	TL3-01ZK	65.0	75.0	1.3	3.6	0.0	0.0	70	TL13-05ZK	64.4	68.8	0.0	33.3	0.0	0.0
35	TL3-02ZK	77.6	21.3	0.0	9.3	0.0	7.0	71	TL14-01ZK	97.5	8.9	0.0	3.4	0.0	0.0
36	TL3-03ZK	91.1	52.0	0.0	20.0	0.0	0.0	72	TL14-03ZK	84.3	38.0	0.0	38.6	0.0	0.0

Samples renumbered from 1–72 representing the position from west to east geographically. Details refer to Table RD1. Numbers 1–17 are from Zeng et al. (2009)

For indices of heavy minerals, refer to text

distance and source direction, ATi can be used to constrain chemical alteration during temporary storage in intense weathering environments (Morton and Johnsson 1993), and RuZi is able to determine source area variations because rutile and zircon have similar physical and chemical behaviors but different source rocks (Force 1980). Therefore, in this paper, ZTR, ATi, and RuZi are chosen for provenance analysis.

We collected a total of 65 fresh samples of fine- to medium-grained sandstones. Of them, 55 were eligible for heavy mineral analysis (Tables 1, 2) after microscopic inspection. Ten samples were excluded as they were either highly metamorphosed with preferred mineral orientation or they did not have a suitable grain size. Fifty-five samples of this study and 17 samples of former work (Zeng et al. 2009) at Rinbung were analyzed for the index change of

heavy minerals in the study area. Values of the ZTR index were projected on the scaled geological map, and sediment channels were depicted with representations from low to high ZTR values.

Grain counting and Dickinson triplots

To study the tectonic setting of a source area, traditional point counting of the clastic composition of sandstones was carried out under the microscope in order to fill the obtained data into Dickinson triplots, applying the Gazzi–Dickinson standards. For details, refer to Dickinson and Suczek (1979), Ingersoll et al. (1984), and Dickinson (1985). Over 300 grains (and many more points) were counted for each thin section (Table RD2).

Thirty-one sandstone samples were collected for thin-section analyses. These samples are medium- to coarse-grained sandstones (Fig. 3), for which the same grain size is vital regarding the grain counting procedure in order to minimize grain size effects (Ingersoll et al. 1984). Data of this study plus data of former works (Fig. 2; Table RD3) at Qonggyai, Gonggar (Li et al. 2004) and Rinbung (Xu et al. 2009; Li et al. 2010) were combined to be plotted in the Dickinson triplots (Fig. 4) so that the whole data set is representative for the entire Langjiexue Group.

Grain size and lithological thickness

The study of clastic grain size change is important to determine the direction of the source area and the transport pattern. The distribution and dispersal pattern of grain size change provides information on the transport direction and depositional environment. The grain size and bed thickness changes in the clastic rocks were determined with field methods.

The ratio of S/M is employed as the total thickness of sand (S) versus mud (M) to analyze the change in clastic grain size, in which the thickness of "sand" actually is the stratigraphical total thickness of sandstone/graywacke and (argillaceous) siltstone, and the "mud" is the stratigraphical sum thickness of (silty, calcareous, siliceous) slate (shale, mudrock) at one observation stop.

Lithological observations were made at 72 outcrops/observation stops along 15 geological routes (Fig. 2; Tables 1, 4). Thereafter, lithostratigraphic thicknesses were measured and added up for each observation stop. The total thickness of the strata differs from outcrop to outcrop due to different outcrop exposures (Fig. 5), but the total always measures >50 m (usually 80–200 m) per stop. To express the geographic trend of grain size change (i.e., thickness of lithology), the S/M ratio was adopted to draw isolines on the geological map sketch. Values of the S/M ratio were projected on the scaled geological map and linked with the same value to form S/M isolines. Intervals of isolines can vary due to discrepancies of ratios for different parts of the study area. Only submarine fan deposits have been studied as fans show the overall trend of grain size decrease in down-fan direction.

Paleocurrents

Paleocurrent indicators help to establish paleoslope and paleotransport directions, which, in turn, reveal the direction of the source area with respect to the basin. Therefore, a direct application of the method is that the paleocurrent directions have also been used to demonstrate sediment dispersal patterns (e.g., Boggs 2009; Wang and Li 2003). Among the different types of paleocurrent indicators (refer to Selley 2000; Wang and Li 2003), flute casts are the most common and crucial ones for deepwater sediments. The paleocurrent indicators were measured and corrected for tectonic tilt.

There are abundant flute casts in the Langjiexue Group (Fig. 6). 959 paleocurrent indicators were measured at 54 locations in the field (Table 1 and Table RD3). These new data, compiled together with former published data (373 paleocurrents at Qonggyai and Zhanang, Li et al. 2003a; 114 paleocurrents at Rinbung, Xu et al. 2011. Table RD3) were composed to construct rose diagrams with azimuth intervals of 10°, indicating the directions and styles of paleoflows (Fig. 7). The majority of rose diagrams are unimodal in their distribution (compare Tucker 2003). For simplification and clarification, the paleocurrents have been projected on the map by arrows. Each arrow represents a main/focal paleocurrent direction of one rose diagram (of about 10 measurements) from every stop. Therefore, the corresponding paleocurrent map would be representative of the regional sediment dispersal pattern since all of the paleocurrent data were obtained from the same lithofacies (mainly submarine fan channel deposits).

Results and interpretations

Heavy mineral assemblages and indices

A variety of heavy minerals is present within the sandstones of the Upper Triassic Langjiexue Group in southern Tibet. Zircon, rutile, tourmaline, apatite, and anatase are the most common ones in each sandstone sample. Zircon is predominant (˃60 % in general) among most samples (Table RD1). The association indicates polygenetic sources, deriving from sedimentary and/or metamorphic and/or magmatic rocks of the source area.

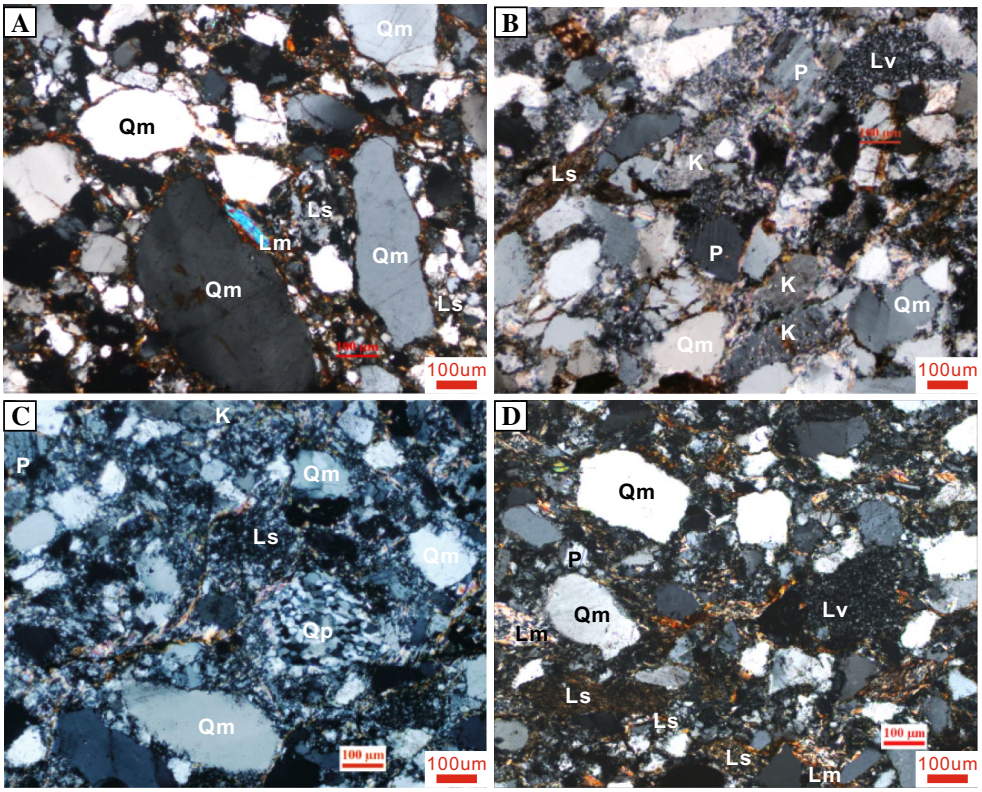

Fig. 3 Microphotographs of sandstones, showing the texture and composition of sandstones from the Langjiexue Group. A, TL11-5a, T_3n; B, TL11-5b, T_3n; C, TL4-3, T_3; D, TL3-1b, T_3 (for details, refer to Table 1). Qm, monocrystalline quartz; Qp, polycrystalline quartz; K, K-feldspar; P, plagioclase; Lv, volcanic clast; Lm, metamorphic lithic clast; Ls, sedimentary lithic clast

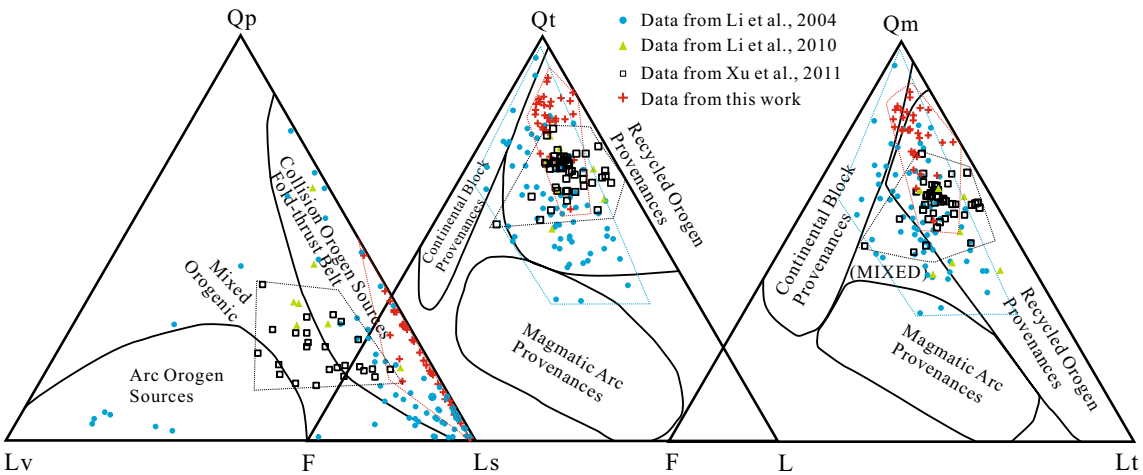

Fig. 4 Dickinson triplots (Dickinson and Suczek 1979; Dickinson 1985) with sandstone composition of the Langjiexue Group. F: feldspar, L: lithic, Lt: total lithics, Ls: sedimentary lithics, Lv: volcanic lithics, Qm: monocrystalline quartz, Qp: polycrystalline quartz, Qt: total quartz. Note that most sandstones fall into the "recycled orogen field" in the Qt–F–L triplot. Some fall into the "recycled orogen" provenance and "mixed" provenance fields in the Qm–F–Lt triplot, and others fall into the "collision orogeny," fold-thrust belt and "mixed orogenic" fields in the Qp–Lv–Ls triplot. Data of former workers refer to supplementary Table RD1

This view of polygenetic sources is corroborated by the occurrence of chrome spinel. In low quantity, chrome spinel (mainly) occurs in samples from the geological routes TL3 to TL5, TL12, and TL13 (Table RD1), likely indicating a basic to ultrabasic magmatic source for the sandstones of the Gonggar-Zhanang and northern Lhunze regions.

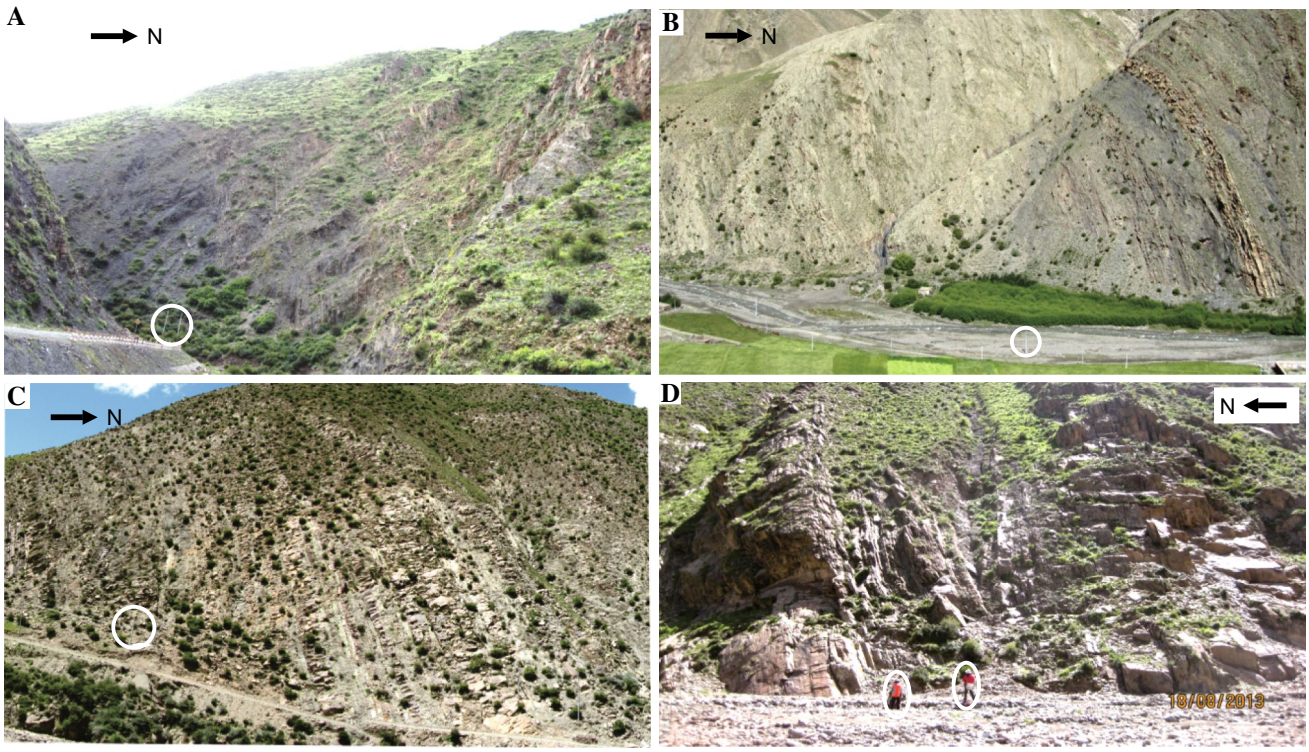

Fig. 5 Field photographs showing different S/M ratios. **a** *Dark gray/black* slate with increasing siltstone and sandstone to the *right*, TL11-01 near Xoisar; **b** thin- to medium-bedded sandstone within the slate sequence, ~15 km west of TL12-01; **c** thin- to medium-bedded sandstone, intercalated with slate near TL4-01; **d** medium- to thick-bedded sandstone, intercalated with slate near TL4-2. Ratios increase from **a** to **d**. Telephone pole in **a**, **b**, and **c** in *white circles* is ~10 m high. For more details of observation sections, refer to Table 1

The ZTR contents are high, ranging from 60 to 98 % and are generally >80 % (Table 2; Fig. 8). High ZTR contents indicate that the clastic sediments of the Langjiexue Group are far-travelled.

ATi values vary greatly from ~5 to 100 %, showing an inversely mirrored attitude of the ZTR values in W–E direction (Table RD1; Fig. 8). To some extent, this may indicate a distance change in source area by intensity of weathering. The shorter the distance is, the lower the weathering degree and the higher the ATi value will be, which is opposite to the ZTR transportation trend.

RuZi values are generally less than 40 %, but vary in three different corresponding zones from the west to the east: light zone, gray zone, and dark zone (Table 2; Fig. 8). They are quite high eastward from Zhanang (>20, 30 % on average; >42 samples), relatively low (most <20 %) between Nagarze (route 1) and Zhanang (route 4), and variable west of Nagarze. This distribution may indicate proximity to a source area of high pressure and a subduction zone east of Zhanang and, again, different source areas for the Langjiexue Group.

In summary, CZi, MZi, and GZi are too low to reveal the characteristics of the source area. But individual samples may have a high value of these indices, except for the above-mentioned Cr (chrome)-spinels (CZi), MZi is relatively high in TL4-5 and TL5-3. It may relate to granites or granitic pegmatites. Garnet (GZi) also rarely appears in some samples (e.g., TL1-001A, TL1-8, and TL2-3), indicating the relationship with metamorphic rocks.

Because the heavy mineral samples are mostly channel sandstones from the submarine fan deposystem (Zhang et al. 2015), ZTR map plots can be used to trace fan channels. As Fig. 9a shows, the double lines show increasing ZTR values toward the south. These double lines could represent channels though not all of them are exactly real. However, the distribution of ZTR values in Fig. 9a does reveal the main direction of sediment dispersal. In the Nagarze area, there may be two main channels, judged by ZTR values increasing from ~80 % via ~92 % to ~95 %, respectively. Between Gonggar and Zhanang, three short channels display relatively high ZTR values in the northern area. Similar trends are seen in two channels between Zhanang and Qonggyai, and a short channel in Zedong as well as in seven channels of the Lhunze area. Channels with low ZTR values may represent channels that had formed at an early stage of fan progradation.

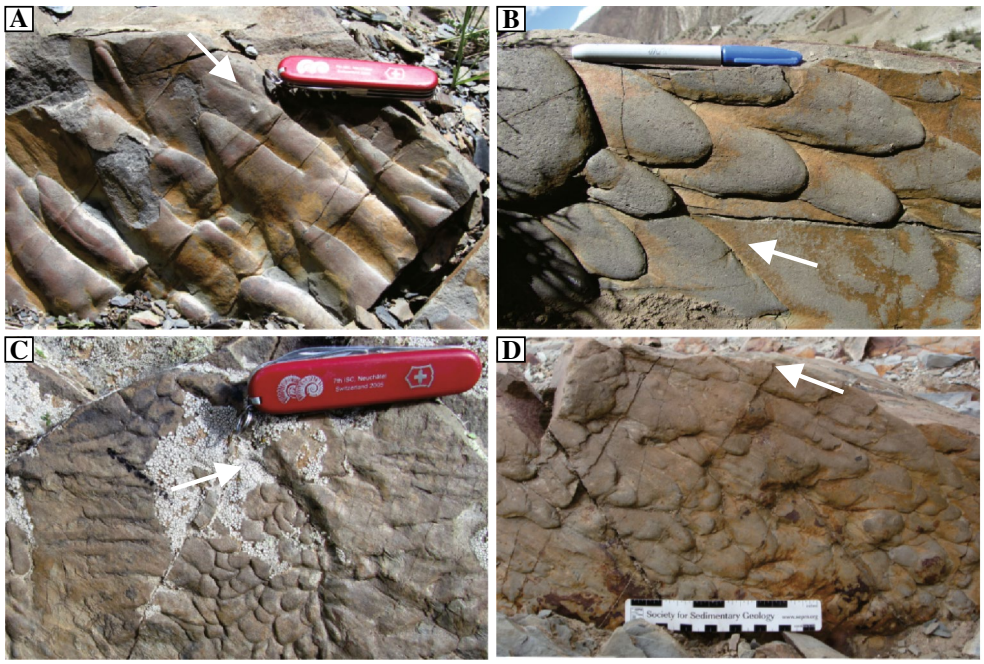

Fig. 6 Photographs of different flute casts. **a** Triangular ("*heel-shaped*") flute casts with a pointed upstream end at ~15 km east of TL12-01, Swiss knife is 9 cm long; **b** rounded upstream end lobate flute casts at TL03-02, pen is 13.8 cm long. **c** Flattened-rounded upstream end flute casts at TL4-2, Swiss knife is 9 cm in length; **d** elongate flute casts with a rounded upstream end at TL2-2, ruler is 20 cm long. *Arrows* point to the main paleocurrent direction

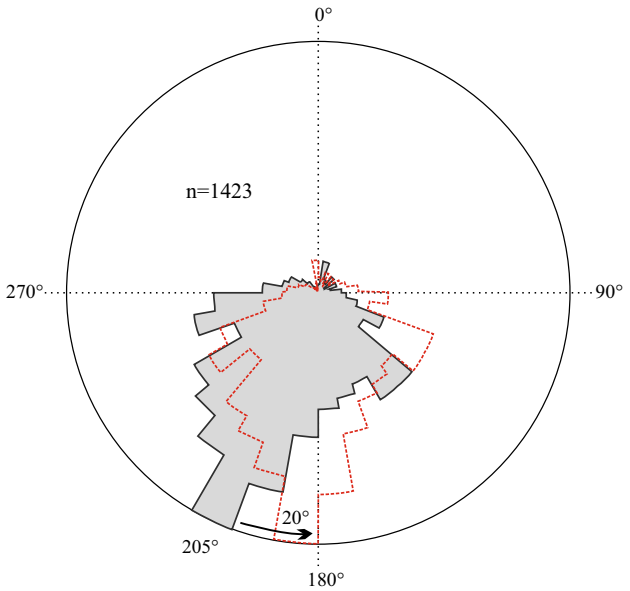

Fig. 7 Rose diagram showing the mean palaeocurrent direction of 205° for the Langjiexue Group. Dotted line with a main direction of 185° is the value for correction of counterclockwise rotation of 20° around a vertical axis (Antolin et al. 2011). The data are from previous studies (Li et al. 2003b; Xu et al. 2011) and this work. For details, refer to Table RD3

Sandstone composition and tectonic settings

Some sandstone samples of medium to high metamorphic grade, exhibiting preferred mineral orientations, were excluded from the compositional analysis as felsic grains may have become dissolved. Other grains may have recrystallized, suffered chemical alteration, and lithic grains may have been disintegrated in the process of metamorphism. Nonmetamorphic and low-grade metamorphic sandstones were selected for grain counting. They are dominated by medium to fine sand grains of feldspar and/or lithic (quartz) sandstone or graywacke. Clayey, calcic (mainly calcite), and iron-bearing (mainly hematite) material may fill interparticle pores (Fig. 3). Quartz (57.3–89.4 %) and other clasts (6.3–27.2 %), e.g., fragments of mudrock, shale/slate/phyllite, and schist, are the main components; feldspars, represented by plagioclase and K-feldspar, are of relatively low abundance (1.0–15.5 %) (Table 3 and Table RD2). Concerning the sandstone maturity, the sandstones are poorly to well sorted (mostly poorly and moderately sorted) and angular to sub-rounded (mostly sub-angular and sub-rounded). In summary, the sandstones reveal the characteristics of relatively low compositional and textural maturity (classification scheme refer to Tucker 2001) (Table RD2).

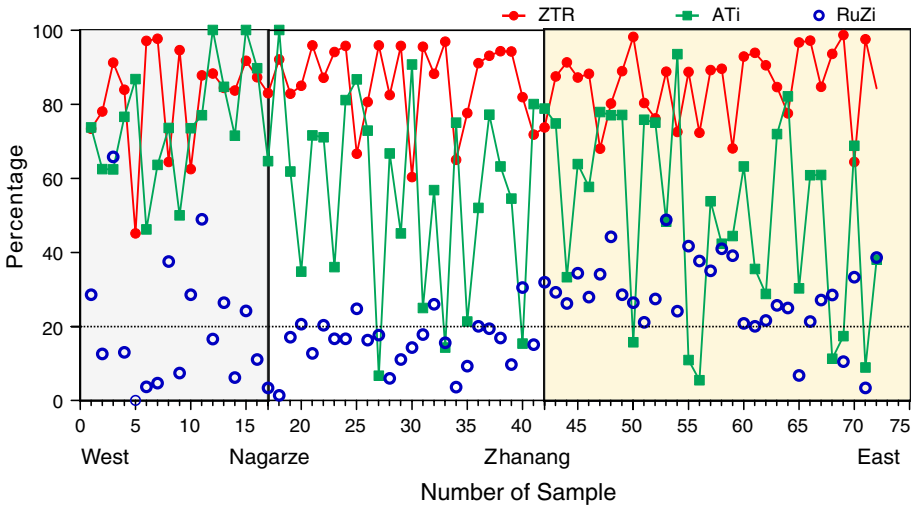

Fig. 8 Diagram showing changes in key heavy mineral composition of the Langjiexue Group from west to east. *Note* ATi values inversely mirror ZTR values. RuZi values are significantly higher in the east and west. Samples are numbered corresponding to their location from west to east, refer to Table 2 and RD 1

The grain counting results are synoptically summarized in Fig. 4. Most of the sandstones fall into the "recycled orogeny" provenance field of the Dickinson Qt–F–L and Qm–F–Lt triplots with some transitions into neighboring fields (Fig. 4). The Qp–Lv–Ls triplot reveals that the sandstones mainly derive from "collision orogen and fold-thrust belt" sources (for details, see the section of "Provenance of components"). However, the transition into other fields again indicates that different geological settings supplied the Shannan Basin with sediment.

Grain size distributions from lithological thickness

Stratigraphic thicknesses of different lithologies were studied and calculated (Fig. 9b; Table 4). The S/M ratios generally decrease from north to south, but they differ in W–E direction (Fig. 9b): 0.18–0.02 in Nagarze; 4.0–1.0 near Xoisar village, Lhunze; 29.0 to only 2.0 in western Zara villages, Lhunze. Also, discrepancies occur in N–S direction (Fig. 9b) with increasing tendencies, possibly caused by channel facies that developed in these areas (Zhang et al. 2015). A southwesterly change from 3 to 0.2 occurs in eastern Shannan; others include 1.86 to 0.2 southward between Qusum and Zedong; 2 to 0.4 of both toward the southeast and southwest between Zedong and Zhanang, 1.86 to 0.33 to the south with few exceptions and 1 to 0.4 again to the areas further south in the vicinity of Gonggar; 1.5 to 0.33 north of Nagarze. The fact that S/M ratios are not always decreased from north to south could be attributed to the alternating progradation and retrogradation of submarine fans.

Paleocurrent directions

Paleocurrent data indicate a dominant southward flow, mainly varying between 120° and 270° with a mean vector of 205° (185° when corrected for counterclockwise rotation of 20°. See Fig. 7 and Antolin et al. 2011). However, there are minor differences from west to east (Fig. 9c). In the Rinbung area, former paleocurrent data direct southeastward and southwestward (Li et al. 2003a, b; Xu et al. 2011). Between Nagarze and Gonggar, paleocurrents are southwestward with a few exceptions to the southeast or south. Between Gonggar and Zhanang, both southeast and southwest directions are present and dominated by southeast paleocurrents. Further east to Qonggyai, the flow was mostly to the southeast. East of Qonggyai, the paleocurrents are mainly southwest-directed with only some local scatter. The paleocurrents indicate a mainly southward paleoflow and a largely uniform sediment dispersal pattern for the Langjiexue Group.

Discussion and conclusions

Radial-curved sediment dispersal pattern

By combining heavy mineral data, S/M ratios, and paleocurrents, a sediment dispersal pattern of the Langjiexue Group is proposed (Fig. 9d). The sediments were transported southward/southwestward by main feeder channels toward the basin floor where they fanned out in the mid-fan and outer-fan areas by distributary channels and channel overflows within a system of several laterally coalescing submarine fans in the sense of Zhang et al. (2015). Three dispersal systems were distinguished in the submarine fan-dominated deep-sea system (Fig. 9d): one is to the east of Zhanang, the second one is between Zhanang and Nagarze, and the third one is to the west of Nagarze. The shape and scale of each depositional body are contoured and depicted by the wave shape of the isolines and different distributions of ratio values.

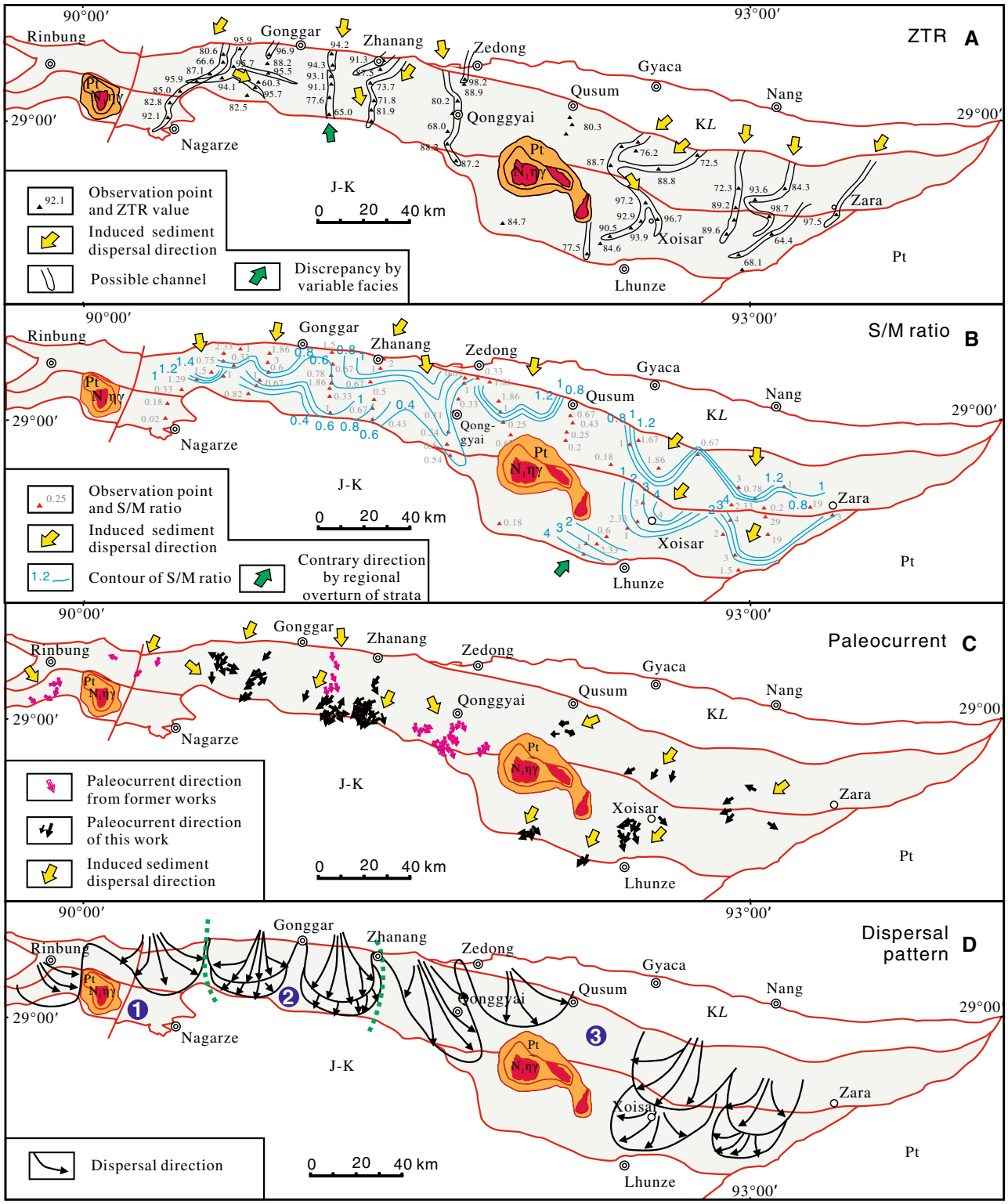

Fig. 9 Distribution map of different sedimentological parameters and dispersal pattern from the Langjiexue Group. **a** ZTR values. Most ZTR values increase from north to south. **b** S/M ratios and isolines. The isoline interval is designated as 1 for the southern part of the Langjiexue Group and as 0.2 for the northern part. **c** Paleocurrent directions. Black arrows are from this work, and the pink ones are from Li et al. (2003b) and Xu et al. (2011). **d** Sediment dispersal pattern. The shape and scale of each depositional body are limited and depicted by the waveshape of the isolines and different distributions of ratio values. *Note* Several sedimentary bodies may fan out and coalesce laterally. For geological symbols and lines, refer to Fig. 2

Table 3 Relative contents of composition ends for Dickinson triplots from sandstones of the Upper Triassic Langjiexue Group in southern Tibet

Sample		Qt-F-L			Qm-F-Lt			Qp-Lv-Ls			Qm-P-K		
		Qt	F	L	Qm	F	Lt	Qp	Lv	Ls	Qm	P	K
1	TL1-6a	57.3	15.5	27.2	54.2	15.5	30.3	10.2	1.0	88.8	77.8	9.8	12.4
2	TL1-06	68.8	12.3	18.8	68.6	10.9	20.6	27.8	0.0	72.2	95.6	2.0	2.4
3	TL1-07	76.1	11.0	12.9	67.6	10.0	22.4	46.1	0.0	53.9	98.7	1.3	0.0
4	TL1-08	79.3	5.6	15.0	79.8	5.8	14.4	6.7	0.0	93.3	97.3	1.6	1.2
5	TL2-1a	69.4	8.8	21.8	73.0	9.4	17.6	32.1	0.0	67.9	86.0	7.0	7.0
6	TL2-01	78.7	9.2	12.1	78.2	10.1	11.7	18.9	0.0	81.1	92.5	4.9	2.6
7	TL2-02	76.5	11.1	12.4	75.7	12.6	11.7	10.3	0.0	89.7	95.5	3.0	1.5
8	TL2-6	70.9	15.1	14.0	62.6	15.1	22.3	37.2	0.0	62.8	80.5	10.3	9.2
9	TL3-1a	76.8	11.6	11.6	72.2	12.0	15.8	20.0	6.0	74.0	90.5	8.7	0.8
10	TL3-1b	77.3	11.5	11.2	74.4	10.5	15.2	16.4	0.0	83.6	90.9	5.4	3.7
11	TL3-1c	70.1	13.4	16.5	74.1	13.3	12.7	22.0	0.0	78.0	89.2	7.1	3.7
12	TL3-2a	84.8	7.5	7.7	83.8	8.1	8.1	25.0	0.0	75.0	95.4	4.0	0.7
13	TL3-2b	82.6	7.1	10.3	79.1	7.2	13.7	16.7	0.0	83.3	89.3	7.4	3.3
14	TL3-05	88.5	4.9	6.6	87.2	5.1	7.8	4.3	0.0	95.7	89.3	8.3	2.4
15	TL4-1a	78.8	7.9	13.2	71.5	7.9	20.5	14.5	8.1	77.4	83.4	9.7	6.9
16	TL4-1b	79.3	7.7	13.1	78.7	8.6	12.7	20.0	0.0	80.0	91.9	4.1	4.1
17	TL4-2	80.3	9.4	10.3	81.9	7.7	10.4	25.6	5.1	69.2	91.7	5.1	3.3
18	TL4-3	89.4	4.2	6.3	86.1	4.6	9.2	28.6	0.0	71.4	94.6	2.9	2.5
19	TL4-6	79.6	9.3	11.2	80.6	9.2	10.2	25.0	0.0	75.0	90.1	7.1	2.8
20	TL5-05	80.5	3.4	16.1	83.7	3.9	12.4	34.3	0.0	65.7	87.7	8.9	3.3
21	TL7-2	85.8	1.0	13.3	90.8	1.0	8.2	8.3	0.0	91.7	90.5	6.8	2.7
22	TL8-2	83.7	2.3	14.0	86.7	2.5	10.8	0.0	0.0	100.0	86.7	6.8	6.5
23	TL10-1	83.6	6.6	9.8	84.6	6.4	9.0	0.0	0.0	100.0	90.7	7.2	2.1
24	TL10-2	84.5	4.0	11.6	87.0	4.1	8.9	0.0	0.0	100.0	87.6	8.9	3.4
25	TL11-1a	83.0	9.9	7.1	73.2	9.3	17.5	17.2	0.0	82.8	93.1	0.0	6.9
26	TL11-1b	83.4	8.9	7.6	66.3	8.3	25.4	14.0	0.0	86.0	88.2	4.7	7.1
27	TL11-3	81.6	10.9	7.6	73.0	10.1	16.9	32.7	0.0	67.3	86.2	7.6	6.2
28	TL11-5a	84.3	8.8	6.9	78.4	8.2	13.4	8.7	0.0	91.3	89.4	4.7	6.0
29	TL11-5b	78.2	12.0	9.7	72.5	9.9	17.6	28.8	0.0	71.2	86.6	7.7	5.8
30	TL15-01	82.7	8.5	8.8	68.7	9.1	22.2	12.1	0.0	87.9	84.3	6.6	9.1
31	TL15-02	80.4	11.4	8.2	70.4	11.6	18.0	28.6	0.0	71.4	86.6	7.1	6.3

Qm = monocrystalline quartz, Qp = polycrystalline quartz, K = K-feldspar, P = plagioclase, Lm = metamorphic lithic grains, Lv = volcanic lithic grains, Ls = sedimentary lithic grains, F = plagioclase + K-feldspar, Ls = Lse + Lm, Lt = total lithic grains = (Lv + Qp + Ls + Lm)

The ZTR contents generally increase southward (Fig. 9a). It is difficult to create isolines for the ZTR values, but it is feasible to link some ZTR values with southward-increasing tendencies to form lines (double lines in Fig. 9a). In agreement with the submarine fan system model and facies observations by Zhang et al. (2015), these lines mainly represent fan channels, enabling southward flow of sediment to the lower fan reaches even though some opposite trends in ZTR values may locally be observed. The channels split up as distributing fan channels and extend as finger-like branches of the main channels.

As shown in Fig. 9b, S/M ratios mainly decrease southward, indicating the presence of finer grain sizes toward the south. The grain size change pattern and shape of isolines are interpreted as an expression of the clastic transport direction, which is the same as deduced for the ZTR values. At a closer look, there are some differences between Rinbung to Qusum on the one hand and eastern areas on the other. S/M ratios decrease southwestward in the east and decrease both toward the southwest and southeast in the region (from Rinbung to Qusum). The overall change displays a radial pattern, to some degree similar to that based on the ZTR data.

The paleocurrents show an overall southward (205°) transport (Fig. 7). At a closer look, one can identify some deviations. In the eastern region, most of the paleocurrent

Table 4 Details on stratigraphic thickness, percentage, and ratio in lithology from the Upper Triassic Langjiexue Group in southern Tibet

No.	Stratigraphic thickness (m) and percentage (%) in lithology						Total thickness	S/M ratio	No.	Stratigraphic thickness (m) and percentage (%) in lithology						Total thickness	S/M ratio
	Slate	Percent	Siltstone	Percent	Sandstone	Percent				Slate	Percent	Siltstone	Percent	Sandstone	Percent		
TL1-001A	197	98.3	1.5	0.8	2	1.0	200	0.02	TL6-01B	80	80.0	5	5.0	15	15.0	100	0.25
TL1-001B	85	85.0	5	5.0	10	10.0	100	0.18	TL6-02	35	70.0	5	10.0	10	20.0	50	0.43
TL1-01	90	75.0	10	8.3	20	16.7	120	0.33	TL6-03	18	60.0	4	13.3	8	26.7	30	0.67
TL1-02	35	43.8	15	18.8	30	37.5	80	1.29	TL7-01	25	50.0	10	20.0	15	30.0	50	1.00
TL1-03	120	40.0	60	20.0	120	40.0	300	1.50	TL7-02	15	37.5	5	12.5	20	50.0	40	1.67
TL1-04	50	50.0	35	35.0	15	15.0	100	1.00	TL8-01	35	35.0	5	5.0	60	60.0	100	1.86
TL1-05	45	75.0	5	8.3	10	16.7	60	0.33	TL8-02	30	60.0	5	10.0	15	30.0	50	0.67
TL1-06	40	57.1	15	21.4	15	21.4	70	0.75	TL9-01	85	85.0	5	5.0	10	10.0	100	0.18
TL1-07	45	30.0	20	13.3	85	56.7	150	2.33	TL10-01	50	25.0	30	15.0	120	60.0	200	3.00
TL1-08	50	50.0	10	10.0	40	40.0	100	1.00	TL10-02	15	30.0	5	10.0	30	60.0	50	2.33
TL2-01	55	55.0	15	15.0	30	30.0	100	0.82	TL10-03	10	20.0	10	20.0	30	60.0	50	4.00
TL2-02	30	60.0	10	20.0	10	20.0	50	0.67	TL10-04	20	33.3	5	8.3	35	58.3	60	2.00
TL2-03	15	50.0	10	33.3	5	16.7	30	1.00	TL10-05	25	25.0	15	15.0	60	60.0	100	3.00
TL2-04	50	62.5	10	12.5	20	25.0	80	0.60	TL10-06	60	40.0	50	33.3	40	26.7	150	1.50
TL2-05	25	25.0	25	25.0	50	50.0	100	3.00	TL11-01	30	30.0	15	15.0	55	55.0	100	2.33
TL2-06	35	35.0	35	35.0	30	30.0	100	1.86	TL11-02	25	50.0	10	20.0	15	30.0	50	1.00
TL3-01	50	50.0	15	15.0	35	35.0	100	1.00	TL11-03	25	62.5	5	12.5	10	25.0	40	0.60
TL3-02	75	75.0	10	10.0	15	15.0	100	0.33	TL11-04	15	30.0	10	20.0	25	50.0	50	2.33
TL3-03	35	35.0	10	10.0	55	55.0	100	1.86	TL11-05	20	20.0	30	30.0	50	50.0	100	4.00
TL3-04	45	56.3	10	12.5	25	31.3	80	0.78	TL11-06	3	20.0	4	26.7	8	53.3	15	4.00
TL3-05	30	60.0	5	10.0	15	30.0	50	0.67	TL11-07	25	25.0	5	5.0	70	70.0	100	3.00
TL3-06	60	40.0	30	20.0	60	40.0	150	1.50	TL12-01	85	85.0	5	5.0	10	10.0	100	0.18
TL4-01	70	70.0	20	20.0	10	10.0	100	0.43	TL13-02	45	56.3	5	6.3	30	37.5	80	0.78
TL4-02	120	60.0	30	15.0	50	25.0	200	0.67	TL13-03	25	83.3	4.5	15.0	0.5	1.7	30	0.20
TL4-03	200	66.7	25	8.3	75	25.0	300	0.50	TL13-04	1	3.3	4	13.3	25	83.3	30	29.00
TL4-04	180	60.0	40	13.3	80	26.7	300	0.67	TL13-05	2	5.0	5	12.5	33	82.5	40	19.00
TL4-05	15	50.0	5	16.7	10	33.3	30	1.00	TL14-01	50	25.0	30	15.0	120	60.0	200	3.00
TL4-06	10	33.3	5	16.7	15	50.0	30	2.00	TL14-02	1	5.0	4	20.0	15	75.0	20	19.00
TL5-01	65	65.0	15	15.0	20	20.0	100	0.54	TL14-03	10	50.0	2	10.0	8	40.0	20	1.00
TL5-02	200	66.7	30	10.0	70	23.3	300	0.50	TL15-01	135	75.0	25	13.9	20	11.1	180	0.33
TL5-03	130	65.0	20	10.0	50	25.0	200	0.54	TL15-02	70	35.0	30	15.0	100	50.0	200	1.86
TL5-04	90	90.0	10	10.0	0	0.0	100	0.11	TL15-03	70	35.0	40	20.0	90	45.0	200	1.86
TL5-05	150	75.0	10	5.0	40	20.0	200	0.33	TL15-04	100	50.0	50	25.0	50	25.0	200	1.00

Table 4 continued

No.	Stratigraphic thickness (m) and percentage (%) in lithology						Total thickness	S/M ratio	No.	Stratigraphic thickness (m) and percentage (%) in lithology						Total thickness	S/M ratio
	Slate	Percent	Siltstone	Percent	Sandstone	Percent				Slate	Percent	Siltstone	Percent	Sandstone	Percent		
TL5-06	50	50.0	10	10.0	40	40.0	100	1.00	TL15-05	80	80.0	10	10.0	10	10.0	100	0.25
TL5-07	60	60.0	10	10.0	30	30.0	100	0.67	TL15-06	150	60.0	20	8.0	80	32.0	250	0.67
TL6-01A	25	83.3	1	3.3	4	13.3	30	0.20	TL15-07	150	50.0	110	36.7	40	13.3	300	1.00

directions point to the southwest, and in the western region, most of the paleocurrent directions point to the southeast. However, in the central region, paleocurrents are directed to both the southwest and southeast (Fig. 9c). The flow pattern is consistent with that of radial-curved fans (compare Mattern 2005), yet a few paleocurrents ensued to the east, west, northwest, and northeast (Fig. 9c). This was attributed to channel lateral migration, channel overflow/flow stripping, and/or channel avulsion with related crevasse channels in the outer part of the inner or middle fan (Li et al. 2003b). A relatively narrow range of paleoflow direction may represent major submarine conduits (Poursoltani et al. 2007) at most measurement points.

The above three parameters demonstrate that the Langjiexue Group has a radial-curved dispersal of sediment (Fig. 9d). The dispersal pattern probably matches a submarine fan deposystem, being consistent with the lithofacies (Zhang et al. 2015). Individual fans laterally overlap in their nonchannelized outer parts (Fig. 10) on the ocean floor and thus constitute a coalescing fan system sensu Mattern (2005). However, differences appear in some local places. Especially in the south of Gonggar and Zhanang (Fig. 9d), the ZTR index seems to be increasing from south to north in the area south of Gonggar and S/M ratios don't decrease continuously from north to south. These differences may be caused by the development of channel facies in these areas (Zhang et al. 2015) and the progradation or retrogradation of the fans.

Provenance of components

The observed heavy mineral assemblages (Table RD1) suggest different source areas for the Langjiexue Group. The source areas were predominantly comprised of sedimentary rocks and granitoids as indicated by the prevalent presence of both well-rounded and euhedral zircons. Other heavy minerals such as pyroxene and chrome spinel point to basic and ultrabasic sources. Garnet and epidote likely reflect metamorphic source rocks. Differences in the RuZi ratio in the west and east (Fig. 8) may be due to lithological variations in the source areas. The different RuZi ratios in the Rinbung area may be due to more than two distinct source areas.

The Dickinson's triplots of sandstone composition illustrate that the Langjiexue Group largely derived from one (or more) recycled orogen(s) (Fig. 8). In general, recycled orogens are dominantly represented by sedimentary strata, subordinate metamorphic and magmatic rocks, exposed to erosion by the orogenic uplift of foldbelts and thrust sheets (Dickinson and Suczek 1979; Dickinson 1985). For the Langjiexue Group, the Qp–Lv–Ls triplot points to a collision orogen rather than a subduction complex or a foreland uplift. For the special population of detrital zircons with

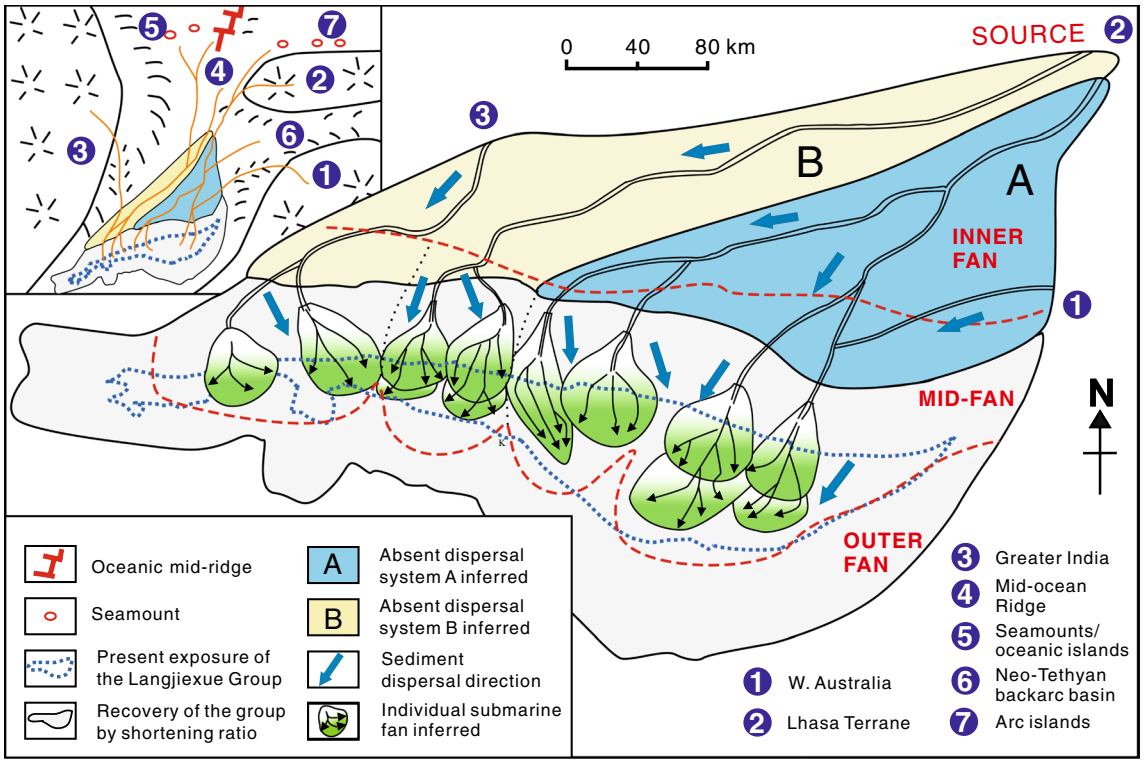

Fig. 10 Dispersal and depositional model of the remnant basin for the Upper Triassic Langjiexue Group. The *insert* at the *top left* corner shows the possible relationships of the basin to sources. The submarine fan system and recovery of stratal width were modified from Zhang et al. (2015)

U–Pb isotope ages of 600–450 Ma in the Shannan Basin (Li et al. 2016), the Pan-African Orogeny that is recognized in the Lhasa Terrane, Australia, and India could be the potential source. The population of detrital zircons with U–Pb isotope ages of 300–200 Ma (Li et al. 2016) could be ascribed to the Permian–Triassic Sumdo Orogenic Belt within the Lhasa Terrane.

Although our present data and former ones (Li et al. 2004; Xu et al. 2011; Li et al. 2010) are from the same area, slight differences can be detected when exact sample locations are considered. Most former works were carried out in the west, whereas our new data derive from farther east. Our results show a more mature composition with a minor share of volcanic lithic fragments and may imply that more continental material was supplied to the east, illustrating different provenance settings in the west and east.

Regarding the provenance setting, Li et al. (2004) first put forward the hypothesis that a block or microplate located between the Indian Subcontinent and the Lhasa Terrane might have provided the material for the Langjiexue Group during the late Triassic. Subsequently, some researchers (Xu et al. 2009; Zeng et al. 2009; Xu et al. 2011) proposed that the source has been the Lhasa Terrane, based on the analyses of sandstone compositions, paleocurrent directions, geochemistry, and heavy minerals from Rinbung County. Investigations of Nd isotopic compositions of bulk rocks (sandstone, phyllite, and graywacke) in Qonggyai County also suggested that the Late Triassic strata were derived from the Lhasa Terrane in the north (Dai et al. 2008). Hf isotopes and the geochronology of detrital zircons from Rinbung suggested a northern derivation (Li et al. 2010, 2014; Webb et al. (2013), supporting this viewpoint, but this was challenged by new evidences of U–Pb isotope dating and Hf isotope of the ~400–280 Ma detrital zircons and the geochemistry of Cr-spinels (Li et al. 2016). Contents of TiO_2, Al_2O_3, Cr_2O_3, and $Cr^{\#}$ of measured spinels show multiple origins of source rocks, dominated by island arc basalts and peridotites. These new data suggest that the Langjiexue Group may have multiple sources (Li et al. 2016).

Our results, plus those of former works (Li et al. 2004; Zeng et al. 2009; Li et al. 2010; Xu et al. 2011) on both heavy minerals and clastic compositions, favor the interpretation of multiple sources for the Langjiexue Group. As we can see, different heavy mineral assemblages reflect different parent lithologies (Table RD1), and varying compositions of sandstones are the response to different tectonic sources as shown in the Dickinson triplots, including "orogenic," "magmatic arc," and "mixed area" (Fig. 4). These results strongly support that the potential sources could be

the Lhasa Terrane, oceanic (island) arc/seamount, and mid-ocean ridge areas as well as Greater India and Australia (Li et al. 2016). Previous works may not have given these aspects adequate considerations.

Remnant basin model and paleogeography

Turbidite systems of the size of the Langjiexue Group form in deep water (Reading and Richards 1994). In the following discussion of the basin type, we consider (1) the radial-curved dispersal pattern, (2) the multiple sediment sources, (3) the latest advance in the paleogeographic understanding of the Shannan Terrane, involving affinities to Lhasa, India, and Australia (Li et al. 2016), and (4) the partly oceanic sources and corresponding oceanic affinities. We concentrate on at least partly oceanic basin settings. Continental basin types, like a rift basin, are ruled out as they cannot explain the oceanic sources.

A trench setting and an accretionary wedge interpretation can also be precluded due to the absence of corresponding olistoliths for the Langjiexue Group, which is dissimilar to the Late Triassic–Paleogene tectonic mélange of the Xiukang Group (Zhang et al. 2002; Cai et al. 2012; An et al. 2015) and the Late Jurassic–Early Cretaceous ophiolitic mélange to the west of the study area (e.g., Gao and Tang 1984; Girardeau et al. 1985; Malpas et al., 2003; Dubois-Côté et al. 2005). Moreover, trenches fill with sediment concurrent with subduction, which causes syn-depositional folding and thrusting (Einsele 2000). In the Langjiexue Group, this cannot be seen. Instead, the flysch mainly prograded and accumulated in a rather undisturbed, regular fashion.

Among oceanic basin types, an ocean sag basin is ruled out because this kind of basin is characterized by fills whose facies sharply contrast with the observed facies of the Langjiexue Group (Zhang et al. 2015). The contrasting facies typically include basal metal-rich sediments, pelagic limestone, radiolarite, deep-sea clay, and manganese nodules (e.g., Frisch et al. 2011). Marginally and vertically, these pelagic sediments may grade into turbidite sequences (Frisch et al. 2011), but these turbidites are derived from passive margins and don't show the diverse sources, including oceanic sources, that occur in the Langjiexue Group.

It was suggested that the Shannan Basin was an oceanic backarc basin (e.g., Zhu et al. 2011). For such a setting, however, it is difficult to account for the abundant orogen-derived clasts as seen in the Shannan Basin. Moreover, the Shannan Basin lacks a corresponding bidirectional dispersal pattern, and, in addition, oceanic backarc basins are expected to have significant basal and marginal arc detritus (Marsaglia 1995), for which there is no evidence in the Shannan Basin either.

Although the Langjiexue Group is a 800- to 2000-m-thick lithostratigraphic unit, it lacks any signs of a shallowing-up sequence. It also isn't dominated by magmatic arc detritus. On these grounds, it is unlikely that the Shannan Basin represents a forearc basin (compare Busby et al. 1995).

As a rifted continental margin approaches (generally obliquely) a subduction zone, coastal promontories collide first, resulting in diachronous orogenic uplift and erosion. Adjoining remnant ocean basins are the natural repositories for voluminous detritus eroded from the growing orogenic belts (Ingersoll et al. 1995). On the main source side of a remnant ocean basin, collisions had taken place between nonsubductable continental crustal elements of variable sizes and intraoceanic arcs, while the basin's sea floor was typically covered by turbidites, derived predominantly from the adjacent source areas (Busby et al. 1995). These aspects relating to remnant ocean basins seem to be compatible with the characteristics of the Shannan Basin. A shrinking ocean basin, the remnant ocean basin, is our first choice of basin type as it would nicely explain how the Shannan Basin got close to the Lhasa Terrane, Greater India, and Australia (Li et al. 2016), near which oceanic lithosphere was subducted. Once subduction ceased, sediment was able to accumulate continuously and undisturbed on the remaining oceanic lithosphere.

Figure 10 illustrates the tectonic setting, source area, sediment transport direction, and dispersal pattern as well as the basin character. Considering the paleogeography of the Shannan Terrane (Li et al. 2016), it is postulated that the remnant basin had formed between the northeastern part of Greater India and northwestern Australia, being predominantly sourced from its northeastern side, the Lhasa Terrane, and also from oceanic (island) arcs/seamounts and mid-ocean ridge areas within the Paleo-Tethys Ocean. Some materials were also derived from Greater India and West Australia (Fig. 10, inlet).

Independent from us, Cai et al. (2016) very recently proposed a similar paleogeography and provenance for the Shannan Terrane based on sandstone petrography and U–Pb detrital zircon analyses. Dissimilarities include (1) a much larger size of the Shannan Terrane (too large?). (2) It seems that the 20° clockwise vertical-axis rotation of the Shannan Terrane during the Early Miocene (Antolin et al. 2011) was not considered. (3) Cai et al. (2016) rely on paleocurrent data by Li et al. (2003a). Thus, their corresponding depiction is not in harmony with the sediment dispersal pattern and paleocurrent style we newly reconstructed. (4) Both Cai et al. (2016) and Li et al. (2016) demonstrated that populations of detrital zircon ages of the Upper Triassic in the Lazi region are different from those in Shannan, i.e., the so-called Nieru Fm. in Lazi. However, this is not the same stratigraphic unit as the "real" Nieru Fm. in Shannan and Kangmar. The

so-called Nieru Fm. in Lazi belongs to the Tethyan Himalaya, whereas, the real Nieru Fm. in Shannan and Kangmar is part of the Langjiexue Group of the Shannan Terrane. (5) Similar to Li et al. (2010, 2014), Cai et al. (2016) have not mentioned the occurrence of Cr-spinel and, thus, not provided a paleogeographic explanation for its provenance.

Due to the above-mentioned aspects, we prefer the paleogeographic and tectonic model proposed by Li et al. (2016), and, in addition, we propose a new sedimentary model in which sediments were mainly derived from the northeast of the remnant ocean basin (Fig. 10). Major feeder channels traversed the area of the future collision orogen and funneled the eroded sediments to the depositional area. The sediment was dispersed in a fanning-out pattern toward the southwest to form a system of several coalescing submarine fans. The submarine canyon served as the main passage through the continental slope (the sediment bypass zone), funneling sediment downslope, and forming submarine fans. Prograding distributary channels transported the sands and silts close to the basin floor.

Summary

1. Four sedimentological methods were adopted to study the Upper Triassic flysch of the eastern Himalaya Orogen in southern Tibet. A variety of heavy minerals is present within the sandstones, in which zircon, rutile, tourmaline, apatite, and anatase are most common, and zircon is predominant (generally over 60 %). The ZTR values range from 60 % to 98 %, displaying an overall increase to the south. The RuZi values vary in magnitude. They are significantly higher east and west of Zhanang (>20 %) than in the center (mostly <20 %). The majority of the S/M ratios decrease from north to south, suggesting an overall decrease in grain size toward the south. The paleocurrent directions vary between 100° to 260° (main vector 185°, corrected for rotation), displaying curved to radial pattern sensu Mattern (2005). The sandstones are mostly poorly and moderately sorted, sub-angular, and sub-rounded (compare Tucker, 2001) and dominated by fine to medium sand-sized quartz grains (57.3–89.4 %), lithic fragments (6.3–27.2 %), and feldspar grains (1.0–15.5 %).
2. The ZTR values, the isoline patterns of S/M ratios, and the paleocurrents all indicate tendencies of southward/southwestward/southeastward sediment transport, allowing for the proposition of a curved to radial sediment dispersal pattern. The sediment was transported from the north, northwest, or northeast by main channels to the basin floor and fan out in the mid- and outer-fan areas by distributary channels. The paleocurrents seem to mimic the submarine fan channel system.
3. The sandstone compositions largely fall into the "recycled orogenic" and "mixed-arc" fields of the Dickinson's triplots. The heavy mineral assemblages support the triplot results as they point to multiple sources, potential sources being the Lhasa Terrane, oceanic island arc/seamount, and mid-ocean ridge areas as well as Greater India and Australia instead of a single provenance for the Langjiexue Group.
4. Considering the multiple sources, the submarine fan dispersal pattern, the recent advance in understanding the relevant paleogeography as well as a discussion that eliminates other basin types, it is suggested that the Langjiexue Group was formed in a remnant basin adjacent to Lhasa, Australia, and Greater India.

Acknowledgments Yin Wang, Yong Sun, Kai Luo, Wenli Xu, Fengfeng Lu, Nima Ciren, Kun Ma, Qiangba Zhaxi, Junzhang Yue, Xiluo, and Zongyang Jiang are acknowledged for taking part in the field work. We are grateful to reviewer Guangwei Li and one anonymous reviewer for their helpful comments and constructive suggestions. We thank the National Natural Science Foundation of China (NSFC 41072075) and the China Geological Survey (South Zhanang 1:50,000 geological mapping project, 12120113034800) for funding the research.

References

Aikman AB, Harrison TM, Lin D (2008) Evidence for early (>44 Ma) Himalayan crustal thickening, Tethys Himalaya, southeastern Tibet. Earth Planet Sci Lett 274:14–23. doi:10.1016/j.epsl.2008.06.038

An W, Hu XM, Garzanti E (2015) Sandstone provenance and tectonic evolution of the Xiukang Mélange from Neotethyan subduction to India–Asia collision (Yarlung-Zangbo suture, south Tibet). Gondwana Research, online. doi:10.1016/j.gr.2015.08.010

Antolin B, Appel E, Montomoli C, Dunkl I, Ding L, Gloaguen R, El Bay R (2011) Kinematic evolution of the eastern Tethys Himalaya: constraints from magnetic fabric and structural properties of the Triassic flysch in SE Tibet. Geol Soc Lond Spec Publ 349:99–121. doi:10.1144/sp349.6

Boggs S (2009) Petrology of sedimentary rocks. Cambridge University Press, Cambridge, pp 1–600

Busby CJ, Ingersoll RV, Burbank D (1995) Tectonics of sedimentary basins. Blackwell Science, Oxford, pp 1–579

Cai FL, Ding L, Leary RJ, Wang H, Xu Q, Zhang L, Yue Y (2012) Tectonostratigraphy and provenance of an accretionary complex within the Yarlung–Zangpo suture zone, southern Tibet: insights into subduction–accretion processes in the Neo-Tethys. Tectonophysics 574–575:181–192

Cai FL, Ding L, Laskowski AK, Kapp P, Wang H, Xu Q, Zhang L (2016) Late Triassic paleogeographic reconstruction along the Neo-Tethys Ocean margins, southern Tibet. Earth Planet Sci Lett 435:105–114

Chen JH, Ba DZ (1986) *Halobia* fauna from Zedang of South Xizang with a discussion on the *Halobia* assemblages in China. Acta Palaeontol Sin 25:1–9 **(in Chinese with English abstract)**

Chen JH, Yang SQ (1983) *Eleganuculana*, new genus, and some other bivalves from the Upper Triassic of Kangmar in Xizang. Acta Palaeontol Sin 22:355–358 **(in Chinese with English abstract)**

Dai JG, Yin A, Liu WC, Wang CS (2008) Nd isotopic compositions of the Tethyan Himalayan Sequence in southeastern Tibet. Sci China, Ser D Earth Sci 51:1306–1316. doi:10.1007/s11430-008-0103-7

Dickinson WR (1985) Interpreting provenance relations from detrital modes of sandstones. Proven Arenites 148:333–361

Dickinson WR, Suczek CA (1979) Plate tectonics and sandstone compositions. Am Assoc Petrol Geol Bull 63:2164–2182

Dubois-Côté V, Hébert R, Dupuis C, Wang CS, Li YL, Dostal J (2005) Petrological and geochemical evidence for the origin of the Yarlung Zangbo ophiolites, southern Tibet. Chem Geol 214:265–286

Dunkl I, Antolín B, Wemmer K, Rantitsch G, Kienast M, Montomoli C, Ding L, Carosi R, Appel E, El Bay R (2011) Metamorphic evolution of the Tethyan Himalayan flysch in SE Tibet. Geol Soc Lond Spec Publ 353:45–69

Einsele G (2000) Sedimentary basins: evolution, facies, and sediment budget, 2nd edn. Springer, Heidelberg, pp 1–792

Force ER (1980) The provenance of rutile. J Sediment Petrol 50:485–488

Frisch W, Meschede M, Blakey R (2011) Plate tectonics and mountain building. In: Plate tectonics, 1st edn. Hardcover, Springer, Berlin, Heidelberg, pp 149–158

Gansser A (1991) Facts and theories on the Himalayas. Eclogae Geol Helv 84:33–59

Gao YL, Tang YQ (1984) Mélanges in the southern Xizang (Tibet). In: Himalaya Geology Editing Commission (ed) Himalaya geology (II). Geological Publishing House, Beijing, pp 27–44 **(in Chinese with English abstract)**

Girardeau J, Mercier JCC, Cao YG (1985) Origin of the Xigaze ophiolite, Yarlung Zangbo suture zone, southern Tibet. Tectonophysics 119:407–433

Hubert JF (1962) A zircon-tourmaline-rutile maturity index and the interdependence of the composition of heavy mineral assemblages with the gross composition and texture of sandstones. J Sediment Petrol 32:440–450

Ingersoll RV, Bullard TF, Ford RL, Grimm JP, Pickle JD, Sares SW (1984) The effect of grain size on detrital modes: a test of the Gazzi-Dickinson point-counting method. J Sediment Petrol 54:103–116

Ingersoll RV, Graham SA, Dickinson WR (1995) Remnant ocean basins. Tectonics of Sedimentary Basins Blackwell Science, Cambridge, pp 362–391

Li XH, Zeng QG, Wang CS (2003a) Palaeocurrent data: evidence for the source of the Langjiexue group in the Southern Tibet. Geol Rev 49:132–137 **(in Chinese with English abstract)**

Li XH, Zeng QG, Wang CS (2003b) Sedimentary characteristics of the upper Triassic Langjiexue Group in Southern Qingjie, Tibet. Geoscience 17:52–58 **(in Chinese)**

Li XH, Zeng QG, Wang CS, Xie YW (2004) Provenance analysis of the Upper Triassic Langjiexue Group in the Southern Tibet, China. Acta Sedimentol Sin 22:553–559 **(in Chinese with English abstract)**

Li GW, Liu XH, Pullen A, Wei LJ, Liu XB, Huang FX, Zhou XJ (2010) In-situ detrital zircon geochronology and Hf isotopic analyses from Upper Triassic Tethys sequence strata. Earth Planet Sci Lett 297:461–470. doi:10.1016/j.epsl.2010.06.050

Li XH, Wang Y, Xu WL, Sun Y, Kong QY, Zeng QG, Xie YW, Mao GZ, Nima CR, Zhou Y, Liu L (2011) Contrasting the Upper Triassic Flysch Langjixue Group and Nieru Formation in Southern Tibet. Acta Geol Sin 85:1551–1562 **(in Chinese with English abstract)**

Li GW, Sandiford M, Liu XH, Xu ZQ, Wei LJ, Li HQ (2014) Provenance of Late Triassic sediments in central Lhasa terrane, Tibet and its implication. Gondwana Res 25:1680–1689

Li XH, Mattern F, Zhang CK, Zeng QG, Mao GZ (2016) Multiple sources of the Upper Triassic flysch in eastern Himalaya orogen, Tibet, China: implications to paleogeography and paleotectonic evolution. Tectonophysics 666:12–22

Malpas J, Zhou MF, Robinson PT, Reynolds PH (2003) Geochemical and geochronological constraints on the origin and emplacement of the Yarlung Zangbo ophiolites, southern Tibet. Geol Soc Spec Publ 218:191–206

Mange MA, Maurer HFW (1992) Heavy minerals in colour. Chapman & Hall, London, pp 1–147

Marsaglia K (1995) Interarc and backarc basins. Tectonics of sedimentary basins, pp 299–329

Mattern F (2005) Ancient sand-rich submarine fans: depositional systems, models, identification, and analysis. Earth Sci Rev 70:167–202. doi:10.1016/j.earscirev.2004.12.001

Montomoli C, Appel E, Borja A, Dunkl I, El Bay R, Ding L, Gloaguen R (2008) Polyphase deformation history of the "Tibetan Sedimentary Sequence" in the Himalayan chain (South-East Tibet) Himalayan. J Sci 5:91

Morton AC, Hallsworth C (1994) Identifying provenance-specific features of detrital heavy mineral assemblages in sandstones. Sed Geol 90:241–256

Morton AC, Hallsworth CR (1999) Processes controlling the composition of heavy mineral assemblages in sandstones. Sed Geol 124:3–29

Morton AC, Johnsson MJ (1993) Factors influencing the composition of detrital heavy mineral suites in Holocene sands of the Apure River drainage basin, Venezuela. Geol Soc Am Spec Pap 284:171–186

Niu YZ, Jiang BY, Huang H (2011) Triassic marine biogeography constrains the palaeogeographic reconstruction of Tibet and adjacent areas. Palaeogeogr Palaeoclimatol Palaeoecol 306:160–175

Pan GT, Ding J, Yao DS (2004) Geological Mapping illumination (1∶1500000) of Qinghai-Tibet Plateau and Its adjacent area. Chengdu Mapping Publishing House, Chengdu

Poursoltani MR, Moussavi-Harami R, Gibling MR (2007) Jurassic deep-water fans in the Neo-Tethys Ocean: the Kashafrud Formation of the Kopet-Dagh Basin, Iran. Sediment Geol 198:53–74. doi:10.1016/j.sedgeo.2006.11.004

Reading HG, Richards M (1994) Turbidite systems in deep-water basin margins classified by grain size and feeder system. AAPG Bull 78(5):792–822

Searle M, Law R, Jessup M (2006) Crustal structure, restoration and evolution of the Greater Himalaya in Nepal-South Tibet: implications for channel flow and ductile extrusion of the middle crust. Geol Soc Lond Spec Publ 268:355–378

Selley RC (2000) 5-Sedimentary structures. In: Selley RC (ed) Applied sedimentology (2nd ed). Academic Press, San Diego, pp 130–180 doi:10.1016/B978-012636375-3/50006-9

TBGMR (1993) Geology of Tibet Autonomous Region. Geological Publishing House. Geological Publishing House, Beijing, pp 1–707 **(in Chinese with English summary)**

TBGMR (1997) Lithostratigraphy of Tibet Autonomous Region. China University of Geosciences Press, Wuhan, pp 1–302 **(in Chinese with English summary)**

Tucker ME (2001) Sedimentary petrology: an introduction to the origin of sedimentary rocks (3rd version). Blackwell Science, Oxford, pp 1–262

Tucker ME (2003) Sedimentary rocks in the field (3rd version). Wiley, Chichester, p 236

Wang HZ (1983) On the geotectonic units of the Xizang (Tibet) region. Earth Sci 19(1):1–8 **(in Chinese with English abstract)**

Wang CS, Li XH (eds) (2003) Sedimentary basin: from principles to analyses. Higher Education Press, Beijing, pp 1–378 **(in Chinese)**

Wang NW, Liu GF, Chen GM (1983) Regional geologic research of Yamdrok, Tibet Geological corpus of Tibet Plateau (3).

Geological Publishing House, Beijing, pp 1–20 **(in Chinese with English abstract)**

Wang CS, Xia DX, Zhou X, Chen JP, Lu Y, Wang GH, He ZW, Li XH, Wan XQ, Zeng QG, Pubu CR, Liu ZF (1996) Geology between the Indus-Yarlung Zangbo Suture Zone and the Himalaya Mountains, Xizang (Tibet), China. Geological Publishing House, Beijing, pp 1–72

Wang CS, Liu ZF, Hébert R (2000) The Yarlung-Zangbo paleo-ophiolite, southern Tibet: implications for the dynamic evolution of the Yarlung-Zangbo Suture Zone. J Asian Earth Sci 18:651–661

Wang LQ, Pan GT, Ding J, Yao DS (2013) Geological mapping illumination (1:1500000) of Qinghai-Tibet Plateau and its adjacent area. Geological Publishing House, Beijing, pp 1–288 **(in Chinese with English abstract)**

Webb AAG, Yin A, Dubey CS (2013) U-Pb zircon geochronology of major lithologic units in the eastern Himalaya: implications for the origin and assembly of Himalayan rocks. Geol Soc Am Bull 125:499–522

Wu H (1984) Lithostratigraphy of Tibet Autonomous Region: division of northern Tethys Himalaya. Science Press, Beijing, pp 115–119 **(in Chinese with English abstract)**

Xu WL, Li XH, Shu J (2009) Material sources of the Upper Triassic Langjiexue Group in Rinbung, Tibet. Acta Geol Sichuan 29:8–10 **(in Chinese with English abstract)**

Xu WL, Li XH, Wang Y, Zeng QG, Sun Y, Ni MCR (2011) Provenance Analysis of the Upper Triassic Flysch in Renbu Area, Southern Tibet. Geol J China Univ 17:220–230 **(in Chinese with English abstract)**

Yin A, Harrison TM (2000) Geologic evolution of the Himalayan-Tibetan orogen. Annu Rev Earth Planet Sci 28:211–280

Yu GM, Wang CS (1990) Sedimentary geology of the Xizang (Tibet) Tethys. Geological Publishing House, Beijing, pp 1–197 **(in Chinese with English summary)**

Zeng QG, Li XH, Xu W, Nimaciren CY, Pu Q, Li J (2009) Heavy mineral assemblages and provenance analysis of the Upper Triassic in Renbu area, southern Tibet, China. Geol Bull China 28:38–44 **(in Chinese with English abstract)**

Zhang XH, Li DW, Xiao LB, Zhang JY (2002) The discovery of the Cretaceous belemnites in the Triassic Xiukang Group, Saga, Tibet. Earth Sci 27(385):440 **(in Chinese)**

Zhang CK, Li XH, Mattern F, Mao GZ, Zeng QG, Xu WL (2015) Deposystem architectures and lithofacies of a submarine fan-dominated deep sea succession in an orogen: a case study from the Upper Triassic Langjiexue Group of southern Tibet. J Asian Earth Sci 111:222–243

Zhou X, Cao Y, Zhu M (1984) Explanation notes to the plate tectonic lithofacies map of Tibet. China. Geological Publishing House, Beijing, pp 1–47 **(in Chinese with English summary)**

Zhu DC, Chung SL, Mo XX, Zhao ZD, Niu Y, Song B, Yang YH (2009) The 132 Ma Comei-Bunbury large igneous province: remnants identified in present-day southeastern Tibet and southwestern Australia. Geology 37:583–586

Zhu DC, Zhao ZD, Niu Y, Mo XX, Chung SL, Hou ZQ, Wang LQ, Wu FY (2011) The Lhasa Terrane: record of a microcontinent and its histories of drift and growth. Earth Planet Sci Lett 301:241–255. doi:10.1016/j.epsl.2010.11.005